JOURNAL OF GEOPHYSICAL RESEARCH, VOL. 102, NO. B7, PAGES 14,853–14,868, JULY 10, 1997

Dilation of anisotropic rock salt: Evidence from Mount Sedom diapir

Yossef H. Hatzor and Eli P. Heyman

Deichmann Rock Mechanics Laboratory of the Negev, Department of Geological and Environmental Sciences, Ben-Gurion University, Beer-Sheva, Israel

Abstract. The mechanical behavior of bedded rock salt is studied using constant strain rate biaxial tests performed on 24 bedded rock salt samples from Mount Sedom diapir. Careful measurements of elastic parameters in unload-reload loops indicate that they are influenced by confining pressure but are not sensitive to anisotropy. The yield stress is also influenced by confining pressure but not by anisotropy. The stress-strain curve therefore indicates isotropy up to the yield stress. Initiation of dilation marks the onset of dependence of volumetric strain on anisotropy. Major principal compressive stress at dilation ($\sigma_{1,d}$) is at maximum when compression is normal to bedding planes ($\beta = 0°$), the stress decreases with increasing values of β, and minimum values are measured when compression is parallel to bedding planes ($\beta = 90°$). Beyond onset of dilation point the relative dilation with respect to stress difference ($V = |\Delta\varepsilon_v/\Delta(\sigma_1 - \sigma_3)|$; $\sigma_1 > \sigma_{1,d}$; MPa^{-1}) increases with decreasing confining pressure and with increasing β; namely, dilation is intensified with decreasing confining pressure and as the major principal compressive stress direction becomes parallel with bedding plane orientation. Current models for compression-dilation boundary ignore anisotropy and therefore provide site specific solutions but fail to describe general rock salt behaviour. A new empirical model for compression-dilation boundary in anisotropic rock salt, developed for a data set from Mount Sedom, predicts that stress at onset of dilation decreases with decreasing confining pressure and with increasing value of β. The rate of change of $\sigma_{1,d}$ with respect to β decreases with decreasing confining pressure, and the rate of change of $\sigma_{1,d}$ decreases with increasing confining pressure for all values of β.

Introduction

The mechanical behavior of bedded rock salt is studied using biaxial and hydrostatic compression tests on 24 samples from Mount Sedom diapir, performed at a constant strain rate of 10^{-5} s^{-1} and at room temperature, under confining pressures between 0 and 25 MPa. The influence of both confining pressure and bedding plane orientation on the elastic constants, the stress-strain law, the yield stress, and the compression-dilation boundary are analyzed in order to assess the mechanical response of proposed storage caverns at depth.

Mount Sedom, a 10 km long by 2 km wide salt diapir having roots as deep as 5 km, is situated along the western margins of the Dead Sea rift valley (Figure 1). The rock salt consists of beds with interbedded anhydride, marl, sand, and shale layers of the Sedom Formation of Pliocene-Pleistocene age [*Zak*, 1967]. An overall thickness of 2500 m has been measured by *Zak* [1967] for the exposed part of the Sedom Formation. *Frumkin* [1996] has estimated a rate of rise of the order of 6–7 mm/yr.

A unique feature of Mount Sedom rock salt is its inherent anisotropy, derived from it being a sequence of bedded salt layers. The dip of the layered sequence is nearly vertical at the surface, and the inclination decreases somewhat at depth (Figure 2). Any proposed underground opening will therefore experience steeply inclined beds in the side walls and the roof. The influence of bedding plane orientation on both elastic and inelastic behavior is therefore of paramount importance and is explored here.

Paper number 97JB00958.
0148-0227/97/97JB-00958$09.00

Constitutive models for elastic deformation [e.g., *Langer*, 1982] compression-dilation boundary [e.g., *Spiers et al.*, 1988; *Ratigan et al.*, 1991; *Cristescu and Hunsche*, 1992] and for failure [e.g., *Pfeifle et al.*, 1981; *Cristescu*, 1993] of rock salt are typically expressed in terms of elastic constants, temperature, stress invariants, and empirical fitting parameters. Rock salts, however, are inherently anisotropic on all scales, exhibiting well-developed bedding planes [*Djahanguiri and Matthews*, 1983] and preferred orientation of halite crystals [*Carter and Hansen*, 1983]. In brittle rock the effect of anisotropy on strength has been discussed extensively, in particular, the effect of discontinuity orientation on stress difference at failure [e.g., *Jaeger and Cook*, 1979; *Hoek*, 1983]. In rock salt, although planar discontinuities in the form of bedding plane partings are abundant, the effect of anisotropy on strength and deformation has been largely overlooked.

The constant strain rate tests discussed here are used to study the effect of anisotropy (bedding planes), using samples which were loaded at different angles between the major principal stress (σ_1) and the upward normal of the discontinuity (β). Ten samples were loaded normal to bedding ($\beta = 0°$), 10 samples were loaded parallel to bedding ($\beta = 90°$), and four samples were loaded at oblique angles to bedding ($27° < \beta < 41°$). It is shown that while elastic deformation is typically isotropic, initiation of inelastic deformation and the relative dilation are clearly a function of bedding plane orientation.

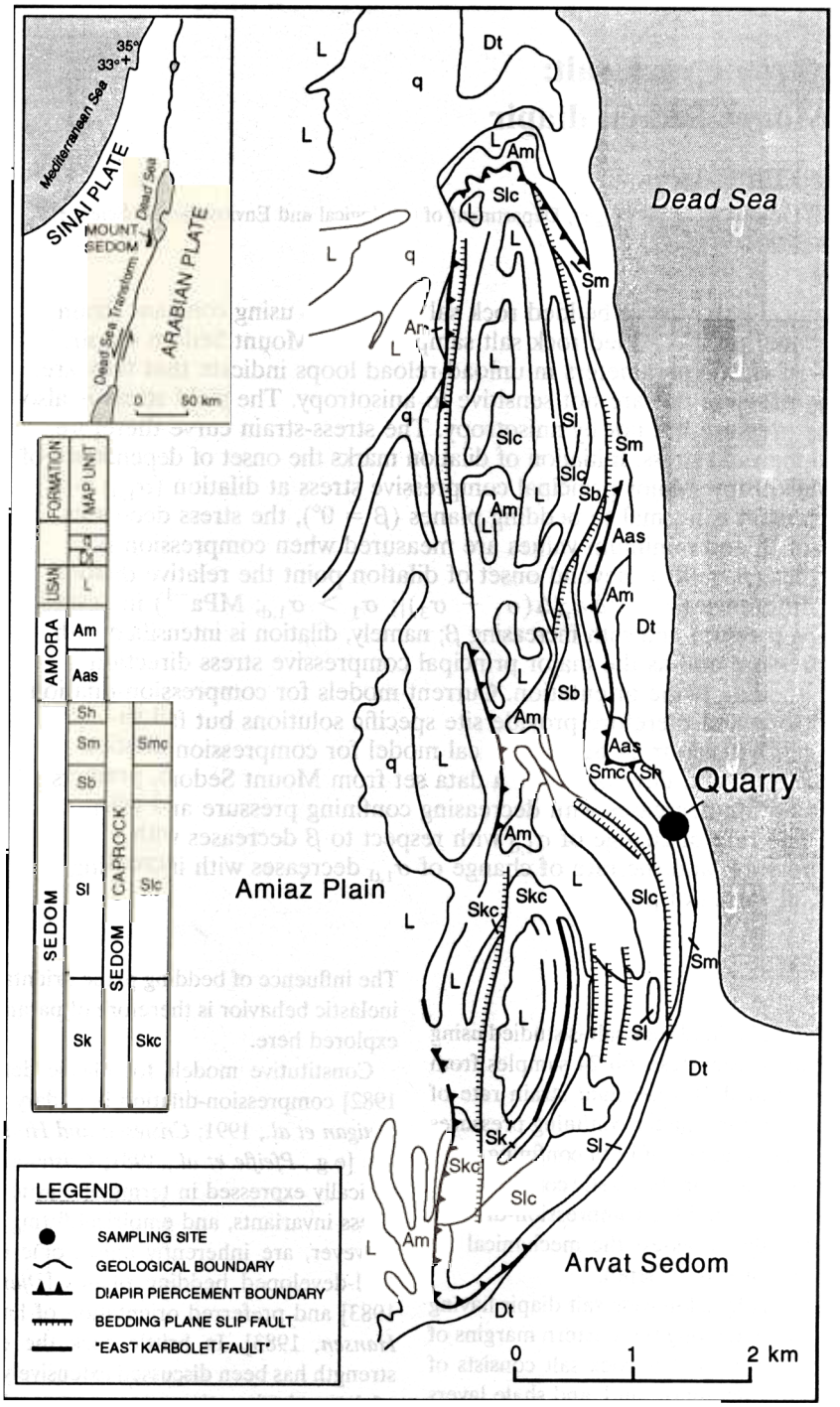

Figure 1. Structure of Mount Sedom rock salt diapir [after *Zak and Freund*, 1980].

Experimental Procedures

Sampling and Sample Preparation

Sampling was performed on five blocks which were separated from the diapir in a quarry (Figure 1). The direction of the normal to bedding was clearly marked in the field on all blocks, since in some cases the blocks appeared completely isotropic. In the laboratory, 24 cylinders were drilled at different orientations from the five blocks, to a nominal diameter of 54 mm and L to D ratio of about 2. The ends were ground to flatness of 0.1 mm using a horizontally mounted disk on a drill press. When roughness was greater than 0.1 mm, the end faces were coated with a thin epoxy layer and then ground using a high-precision surface grinder to a flatness of 0.01 mm (measured on the epoxy coating). The cooling fluid which has been used was kerosene in order to avoid corrosion of equipment.

There were many technical problems associated with sample preparation. Several samples broke during the preparation procedure, some swelled during drilling, others separated across bedding plane partings due to the presence of the cooling fluid.

Following preparation samples were preserved horizontally in a storage room, and encompassed in a soft tissue until testing. Each sample received the initials MS for Mount Sedom.

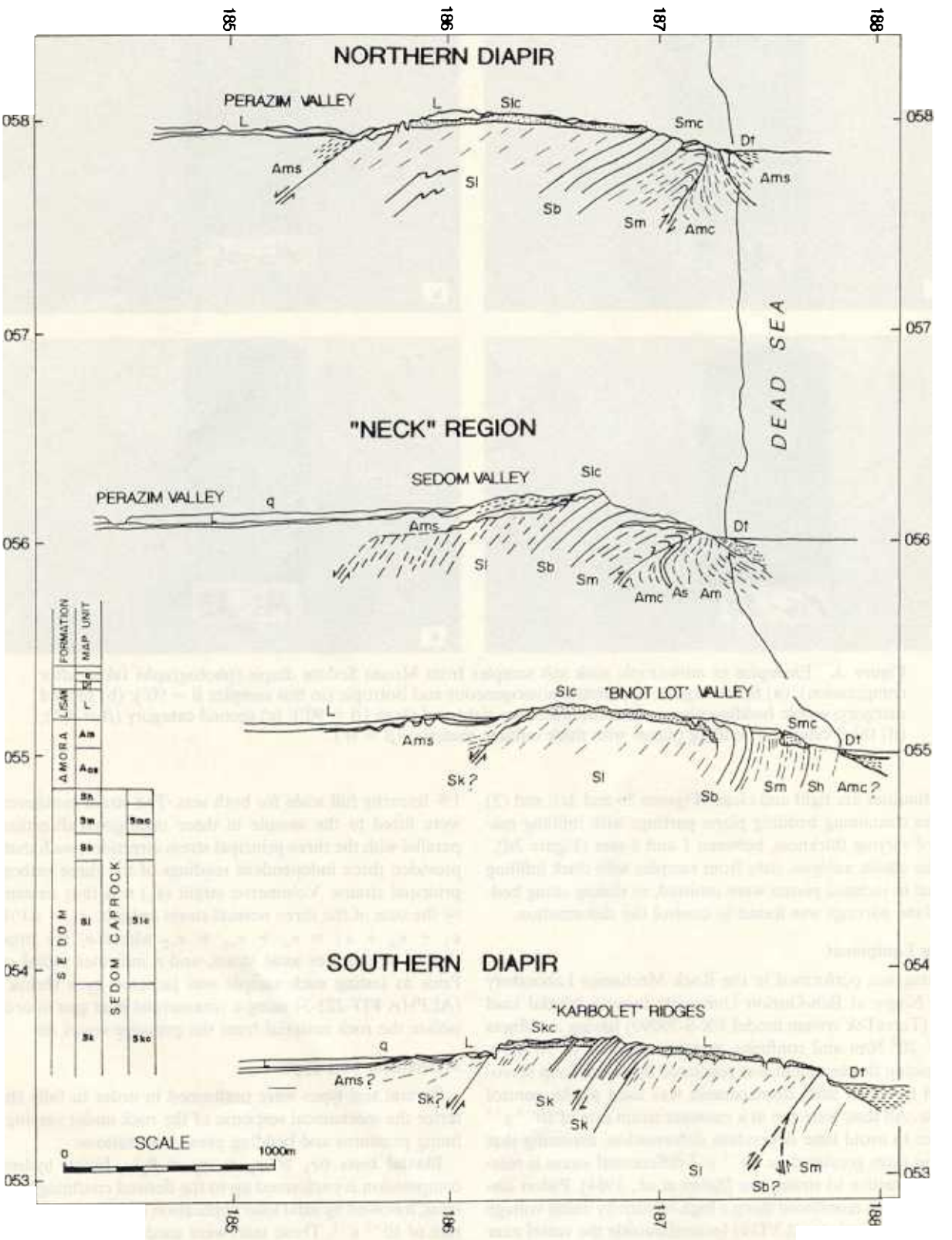

Figure 2. Cross sections along Mount Sedom rock salt Diapir [after *Zak*, 1967]

Description of Tested Samples

The samples can be classified into three main categories: (1) Samples of apparently homogeneous and isotropic rock salt; in this category no bedding planes can be detected in a hand specimen, although the block from which they were prepared was removed from a sequence of subvertical rock salt beds (Figure 3a); (2) samples of rock salt containing visible bedding plane partings, but no infilling material can be detected and the

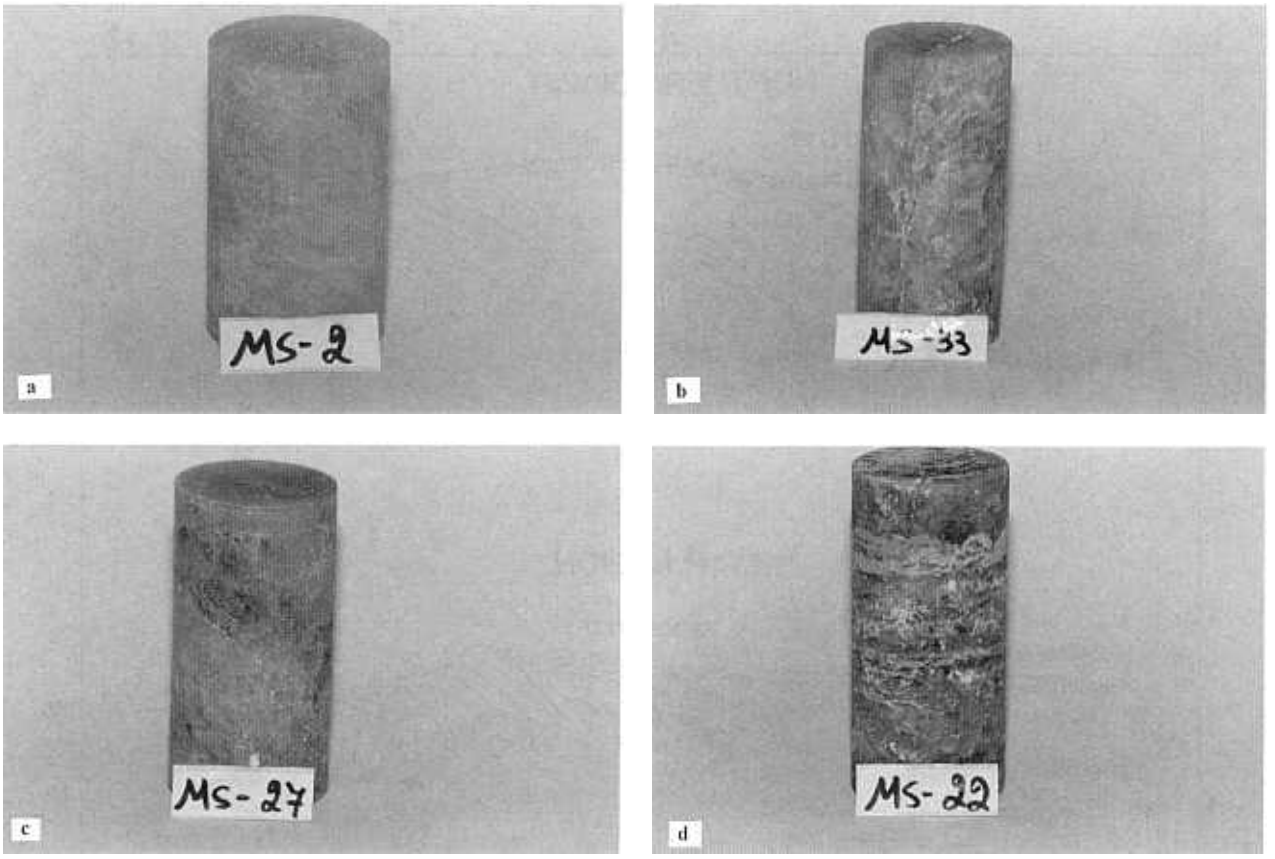

Figure 3. Examples of anisotropic rock salt samples from Mount Sedom diapir (photographs taken after compression): (a) first category, apparently homogeneous and isotropic (in this samples $\beta = 90°$); (b) second category, visible bedding planes, discontinuities are tight and clean ($\beta = 90°$); (c) second category ($\beta = 40°$); (d) third category, bedding planes with thick infilling material ($\beta = 0°$).

discontinuities are tight and clean (Figures 3b and 3c); and (3) Samples containing bedding plane partings with infilling material of varying thickness, between 1 and 8 mm (Figure 3d).

In the elastic analysis, data from samples with thick infilling material in inclined planes were omitted, as sliding along bedding plane partings was found to control the deformation.

Testing Equipment

Testing was performed in the Rock Mechanics Laboratory of the Negev at Ben-Gurion University using a triaxial load frame (TerraTek system model FX-S-33090) having a stiffness of 5×10^9 N/m and confining pressure capacity of 70 MPa. Axial piston displacement was regulated by closed-loop servo-control in which axial displacement was used as the control variable. All tests were ran at a constant strain rate of 10^{-5} s^{-1} in order to avoid time dependent deformation, assuming that at strain rates greater than 10^{-7} s^{-1} differential stress is relatively insensitive to strain rate [*Spiers et al.*, 1984]. Piston displacement was monitored using a high-sensitivity linear voltage differential transducer (LVDT) located outside the vessel near the piston. Load was measured by a sensitive load cell located at the base of the sample stack having a maximum capacity of 222 kN and linearity of 0.5% full scale. Sample axial and radial strains were recorded using four arm axial and transverse strain cantilever sets, where arm deflection was calibrated to displacement (calibration was performed prior to testing). The four-arm axial cantilever set has a 10% strain range and the two four-arm radial sets have a strain range limit of 7%, with 1% linearity full scale for both sets. The strain cantilever sets were fitted to the sample in three orthogonal directions, in parallel with the three principal stress directions, such that they provided three independent readings of the three orthogonal principal strains. Volumetric strain (ε_v) was thus determined by the sum of the three normal strain outputs: $\varepsilon_v = \Delta V/V_0 = \varepsilon_1 + \varepsilon_2 + \varepsilon_3 = \varepsilon_a + \varepsilon_{r1} + \varepsilon_{r2}$ where ε_i are principal strains, a indicates axial strain, and r indicates radial strain. Prior to testing each sample was jacketed by a shrink tube (ALPHA FIT-221-3) using a commercial heat gun in order to isolate the rock material from the pressure vessel oil.

Mechanical Test Types

Several test types were performed in order to fully characterize the mechanical response of the rock under varying confining pressures and bedding plane orientations:

Biaxial tests ($\sigma_1 > \sigma_2 = \sigma_3 = P_c$). Initial hydrostatic compression is performed up to the desired confining pressure level, followed by axial load application under a constant strain rate of 10^{-5} s^{-1}. These tests were used to study the influence of confining pressure (P_c) and bedding plane orientation (β) on the stress-strain law.

Segment tests. (1) During the elasto-plastic stage of deformation in a biaxial test, a loop is performed in which axial stress is unloaded and reloaded at a constant strain rate of 10^{-5} s^{-1}. These tests were used to study the influence of confining pressure and bedding plane orientation on the elastic modulus (E) and Poisson's ratio (ν). (2) During the elasto-

Table 1. Summary of Test Results

Sample	P_c, MPa	E, GPa	ν	$\sigma_{1,d}$, MPa	$\varepsilon_{v,d}$, %	$\sigma_{1,y}$, MPa	$\varepsilon_{a,y}$, %	β, deg
		13.4	0.21					
		17.04	0.28	18.24	0.263			
		12.4	0.213	7.20	0.15	0	0	
		16.64	0.298	28.09	0.136			
		18.6	0.272	17.42	0.05	16.74	0.043	
		16.45	0.319	8.12	0.087	6.74	0.068	
		16.25	0.263	10.88	0.28	8	0.26	
		18.92	0.273	35.59	0.408			
		3.86	0.047					
		7.38	0.648					
		15.47	0.247	6.85	0.1	6.46	0.16	90
		17	0.293					90
		10.86	0.156	7.59	0.135	3.46	0.09	0
		13.02	0.326					0
		4.41	0.387			0.84	0.014	30
		8.2	0.312					30
		15.02	0.256	14.47	0.	10	0.144	90
		18	0.248					90
		18.64	0.26					90
		13.14	0.202	23	0.304	8	0.118	0
		18.54	0.262					0
		14.17	0.251	23	0.328	10	0.144	40
		13.77	0.236	17.26	0.132	10	0.144	30
		17.84	0.357	11.9	0.075	10.2	0.067	90
		19.57	0.323	31.08	0.032	30.40	0.0604	90
		15.45	0.357	4.75	0.020	6.3	0.08	90
		15.32	0.34	6.5	0.055	4.35	0.0537	90
		15.86	0.278	7.4	0.102	4.7	0.097	90
		17.76	0.314	26.07	0.318			0
		19.37	0.338	47.00	0.14	30.7	0.067	0
		18.6	0.283	44.6	0.5	28.20	0.207	0
		14.96	0.316	7.3	0.0445	6.67	0.1156	0
		16.49	0.275	7.4	0.056	4.34	0.053	0
		15.93	0.297	15.3	0.325	5.2	0.1415	0

P_c, confining pressure; $\sigma_{1,d}$, major principal compressive stress at onset of dilation; $\varepsilon_{v,d}$, volumetric strain at onset of dilation; $\sigma_{1,y}$, major principal compressive stress at yield; $\varepsilon_{a,y}$, axial strain at yield; β, angle between upward normal of bedding plane and σ_1.

[a] $\sigma_{3,0} = 15$.

[b] $\sigma_{3,0} = 5$.

plastic deformation stage in a biaxial test, a loop is performed in which axial stress is unloaded at a constant strain rate of 10^{-5} s^{-1}, confining pressure is increased to a new level, and axial stress is reloaded under a constant strain rate of 10^{-5} s^{-1}. These tests were used to study the influence of confining pressure variations on the stress-strain law and to investigate memory aspects. (3) Initial hydrostatic compression is performed up to a desired level ($\sigma_{3,0}$), followed by an unconfined compression test under a constant strain rate of 10^{-5} s^{-1}. These tests were used to study the influence of stress history (or depth of burial) on the stress-strain law.

Experimental Results

A summary of test results for all samples is shown in Table 1. The numbers in parentheses next to the sample name indicate the order of the test in the sequence of segments performed. The confining pressure level was always increased when more then one segment was performed. The reported values of elastic constants are average values, calculated in at least three unload-reload segments at a given confining pressure. The values were found using linear regression along the unloading component of the loop. The yield point, defined by axial stress and axial strain at yield ($\sigma_{1,y}$, $\varepsilon_{v,y}$), marks the departure of the stress-strain curve from linearity, indicating the termination of the linear-elastic stage of deformation. The onset of dilation point, defined by axial stress and volumetric strain at onset of dilation ($\sigma_{1,d}$, $\varepsilon_{v,d}$), was found using the slope reversal point in the total volumetric strain curve, following the convention used by *Brace et al.* [1966]. This point is different from the crack initiation point found by *Martin and Chandler* [1994] for granites by subtracting the elastic volumetric strain from the measured (total) volumetric strain or by detecting the deflection point in the radial strain curve as found for potash salt rock by *Lajtai et al.* [1994].

Stress-Strain Law

A typical stress-strain curve for a biaxial test is shown in Figure 4 for a sample which was loaded in parallel to bedding ($\beta = 90$) under a constant strain rate of 10^{-5} s^{-1}. Three deformation stages can be recognized: (1) elastic stage, terminating at the yield point (point a) and characterized by a linear slope, (2) transition stage, from elastic to elastic-plastic deformation (between points a and b), characterized by a curve with a relatively small radius of curvature, and (3) elastic-plastic stage, governed by strain hardening deformation (between points b and e) and characterized by a curve with a relatively large radius of curvature.

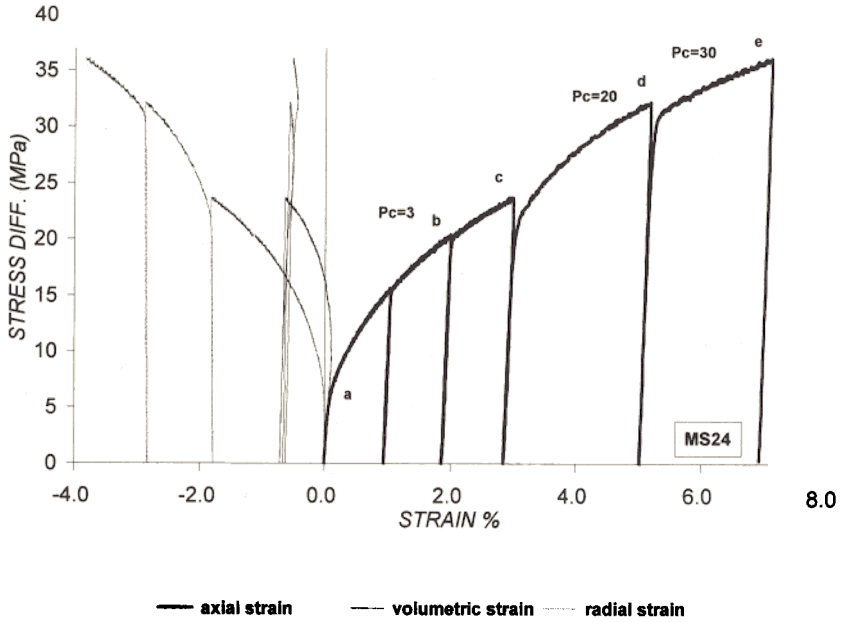

Figure 4. Constant strain rate (10^{-5} s^{-1}) test results for a typical rock salt sample from Mount Sedom which is loaded parallel to bedding ($\beta = 90°$).

Increase of confining pressure at the elastic-plastic stage during an unload-increase confining pressure-reload loop (points c and d) has little effect on the predefined stress-strain law.

The characteristic influence of confining pressure and bedding plane orientation on the stress-strain law is shown in Figure 5 where the results of five biaxial tests performed on samples from block V are plotted. Two tests performed under unconfined compression at $\beta = 0°$ (bold line) and $\beta = 90°$ (dotted line), one test under confining pressure of 4.5 MPa at $\beta = 90°$, and two tests under confining pressure of 24.7 MPa at $\beta = 0°$ (bold line) and $\beta = 90°$ (dotted line) are shown. It can be seen that the strengthening effect of confining pressure is limited to confining pressures between 0 and 4.5 MPa. At higher values of confining pressures the effect on the stress-strain law is negligible. The effect of anisotropy on the stress-strain law is also limited to low confining pressures. Unconfined samples loaded parallel to bedding ($\beta = 90°$) are stronger than samples loaded normal to bedding ($\beta = 0°$); this effect is diminished at higher confining pressures. It is important to note that the anisotropic effect on the stress-strain law at low confining pressure (Figure 5, $P_c = 0$ MPa) is evident only after yield stress has been achieved; during the elastic deformation stage, there is no marked difference in the mechanical response to normal and parallel compression.

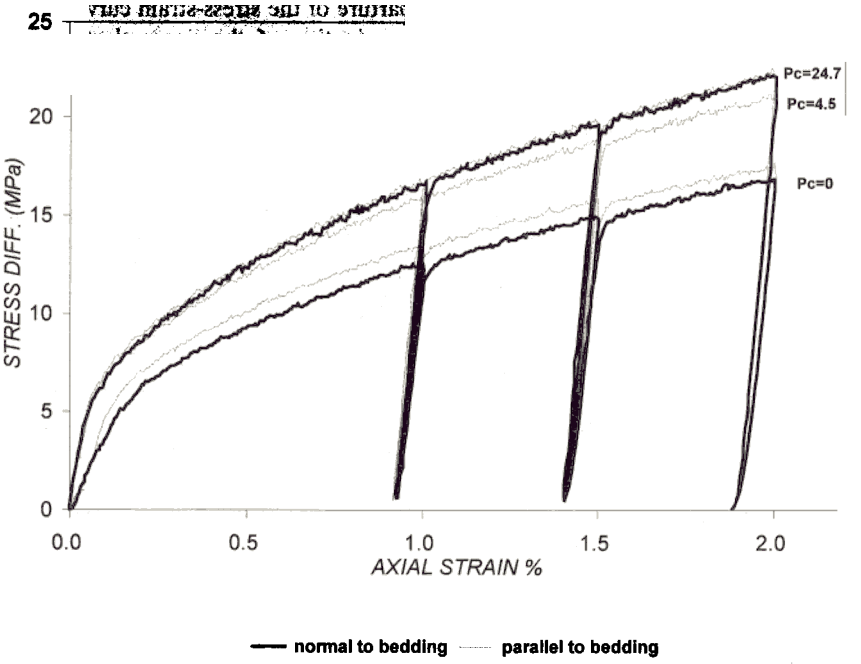

Figure 5. Influence of confining pressure and bedding plane orientation on the stress-strain law.

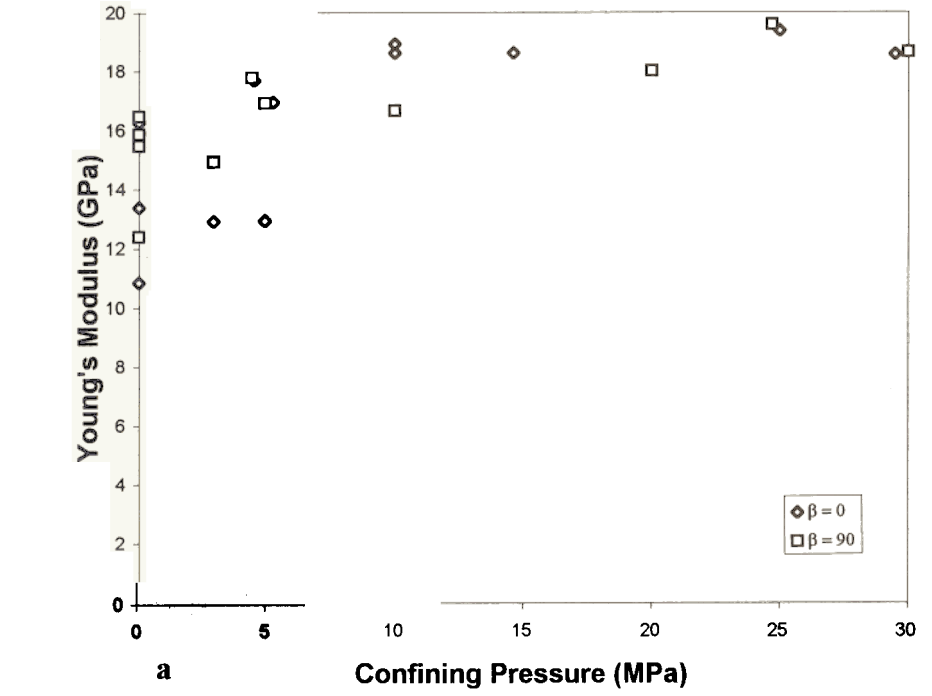

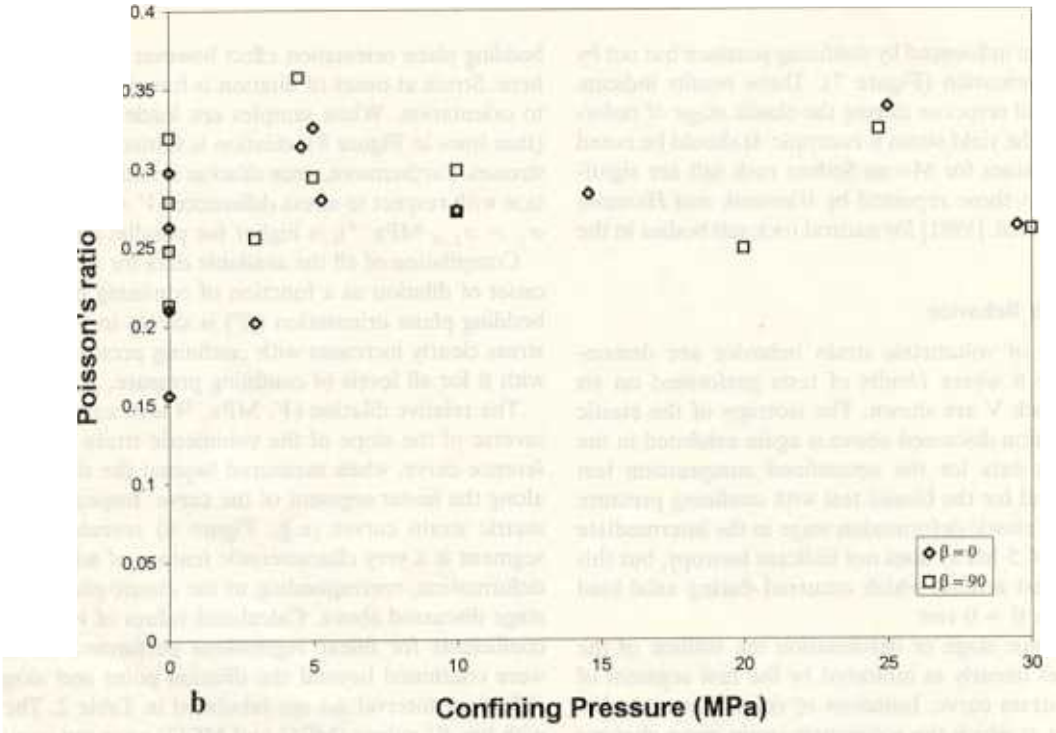

Figure 6. Influence of confining pressure and bedding plane orientation on (a) the elastic modulus and (b) Poisson's ratio.

Elasticity

The influence of confining pressure and bedding plane orientation on the elastic modulus and Poisson's ratio are shown in Figure 6. All the data presented in Table 1 are plotted with the exception of samples containing inclined beds and samples tested following initial confinement. The elastic modulus (Figure 6a) increases with confining pressures in the range of 0 to 10 MPa, beyond which it exhibits a constant value of about 18 GPa. The elastic modulus indicates material isotropy, as samples loaded parallel and normal to bedding exhibit identical results at equal levels of confining pressures. Poisson's ratio appears to be independent of confining pressure at all levels (Figure 6b), exhibiting a constant value of about 0.27. As in the case of the elastic modulus, material isotropy is indicated.

The material isotropy indicated by the elastic parameters is consistent with the isotropy of the stress-strain curve in the elastic stage of deformation (Figure 5). Furthermore, analysis of yield stress data also shows material isotropy, since yield

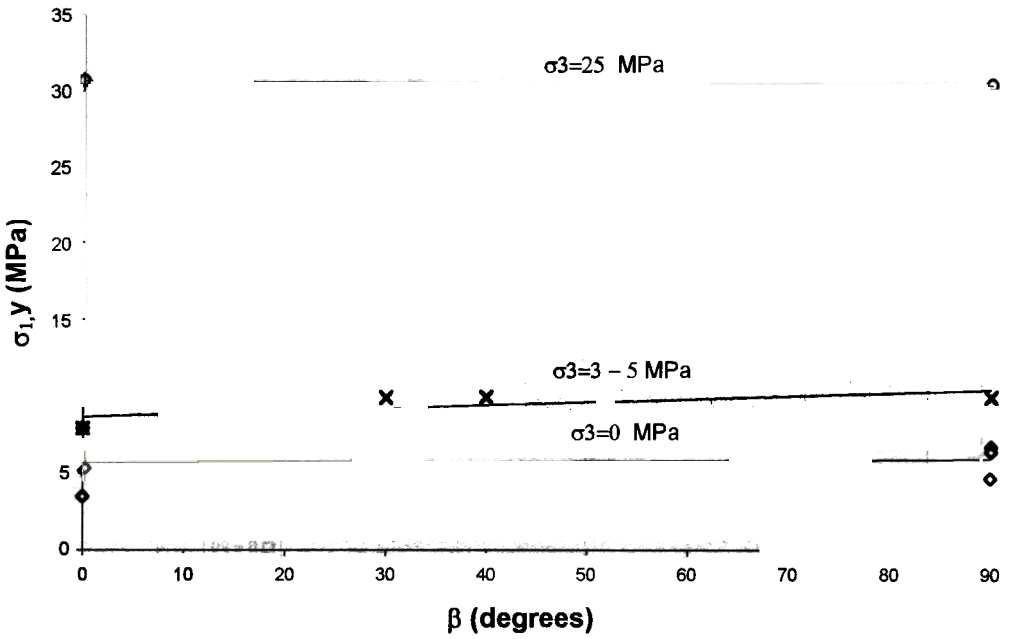

Figure 7. Influence of confining pressure and bedding plane orientation on yield stress. Diamonds, $\sigma_3 = 0$ MPa; crosses, $\sigma_3 = 3$–5 MPa; circles, $\sigma_3 = 25$ MPa.

stress is found to be influenced by confining pressure but not by bedding plane orientation (Figure 7). These results indicate that the mechanical response during the elastic stage of deformation and up to the yield stress is isotropic. It should be noted that yield stress values for Mount Sedom rock salt are significantly higher then those reported by *Wawersik and Hannum* [1980] or *Hansen et al.* [1981] for natural rock salt bodies in the United States.

Volumetric Strain Behavior

Typical trends of volumetric strain behavior are demonstrated in Figure 8 where results of tests performed on six samples from block V are shown. The isotropy of the elastic stage of deformation discussed above is again exhibited in the volumetric strain data for the unconfined compression test ($P_c = 0$ MPa) and for the biaxial test with confining pressure of 24.7 MPa. The elastic deformation stage in the intermediate condition ($P_c = 4.5$ MPa) does not indicate isotropy, but this is a result of a test artifact which occurred during axial load application in the $\beta = 0$ test.

During the elastic stage of deformation the volume of the sample decreases linearly as indicated by the first segment of the volumetric strain curve. Initiation of volume increase begins at the point at which the volumetric strain curve changes sign. At this point the volume of the sample is at a minimum, and this point marks the end of sample compression and the initiation of dilation, i.e., the compression-dilation boundary. From the onset of dilation, deformation is inelastic and volume growth is detected.

Two factors control the volumetric strain curve for biaxial compression under constant strain rate: confining pressure and bedding plane orientation. With increasing confining pressure the amount of compression prior to dilation decreases (or the bulk modulus increases), and the stress at which dilation initiates increases. This dual effect is clearly demonstrated by *Stormont and Daemen* [1992], and by *Stormont et al.* [1992] for New Mexico rock salt, and is found here for all values of β. The bedding plane orientation effect however is new and is explored here. Stress at onset of dilation is found to be highly sensitive to orientation. When samples are loaded parallel to bedding (thin lines in Figure 8), dilation is initiated at relatively lower stresses. Furthermore, once dilation is initiated, the relative dilation with respect to stress difference ($V = |\Delta\varepsilon_v/\Delta(\sigma_1 - \sigma_3)|$; $\sigma_1 > \sigma_{1,d}$; MPa^{-1}), is higher for parallel compression.

Compilation of all the available data for axial stress ($\sigma_{1,d}$) at onset of dilation as a function of confining pressure (σ_3) and bedding plane orientation ($\beta°$) is shown in Figure 9. Dilation stress clearly increases with confining pressure and decreases with β for all levels of confining pressure.

The relative dilation (V, MPa^{-1}) is determined here by the inverse of the slope of the volumetric strain versus stress difference curve, when measured beyond the dilation point and along the linear segment of the curve. Inspection of our volumetric strain curves (e.g., Figure 8) reveals that the linear segment is a very characteristic feature of advanced stages of deformation, corresponding to the elastic-plastic deformation stage discussed above. Calculated values of V and correlation coefficients for linear regressions performed on tests which were continued beyond the dilation point and along a stress difference interval $\Delta\sigma$ are tabulated in Table 2. The two tests with low R^2 values (MS41 and MS42) were not continued well into the linear segment of the volumetric strain versus stress difference curve. The effect of confining pressure and bedding plane orientation on the relative dilation (V) is demonstrated in Figure 10. In Figure 10a the effect of confining pressure on V is shown. In general, the relative dilation decreases with increasing confining pressure and increases with increasing values of β. At low confining pressures the influence of β is very significant; in unconfined compression, the difference is a factor of about 3 ($(V_{\beta=90}/V_{\beta=0})_{\sigma_3=0} \approx 3$). This effect is reduced with increasing confining pressure; at $\sigma_3 = 25$ MPa the difference is about 1.6 ($(V_{\beta=90}/V_{\beta=0})_{\sigma_3=25} \approx 1.6$). The influence of bedding plane orientation on the relative dilation is shown in Figure 10b. Exponential best fit lines are plotted for

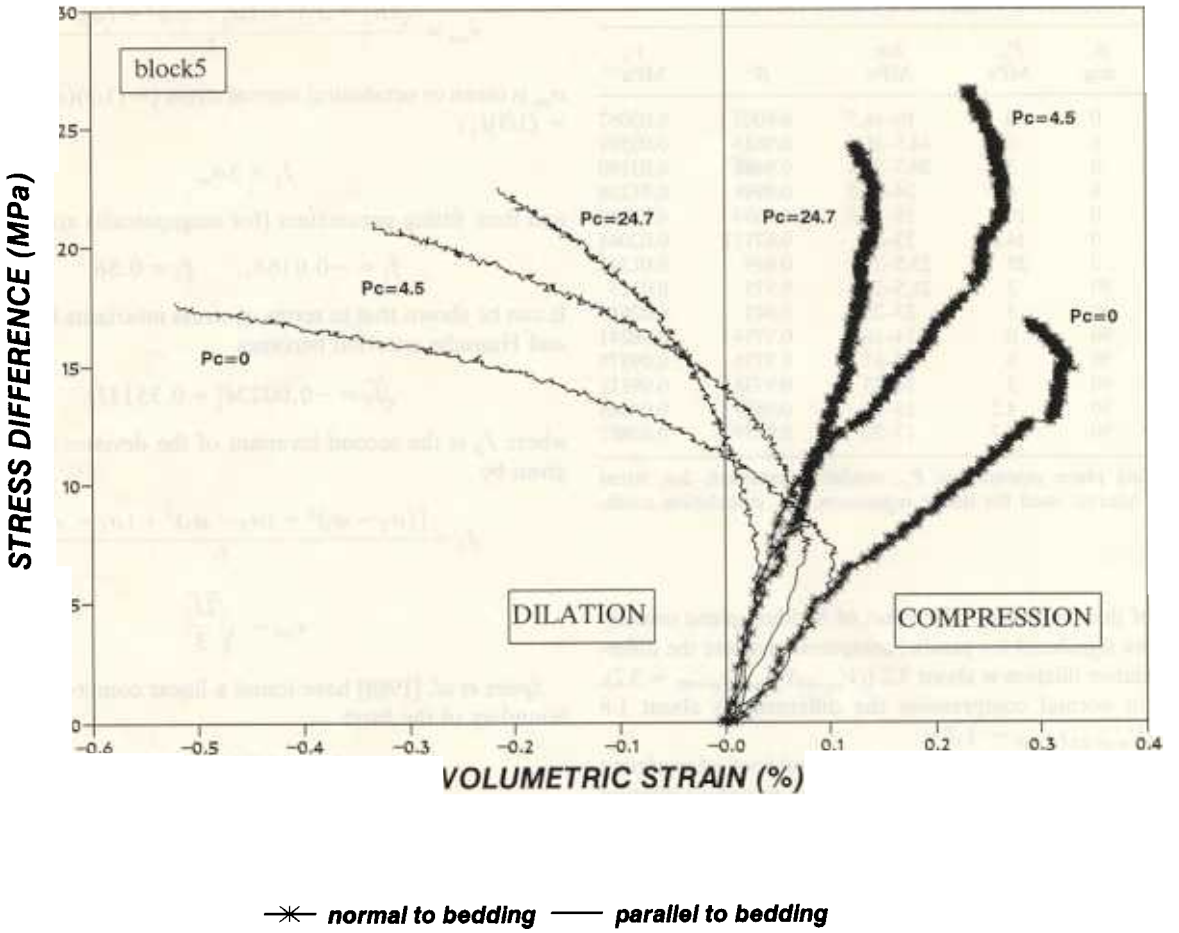

Figure 8. Influence of confining pressure and bedding plane orientation on volumetric strain.

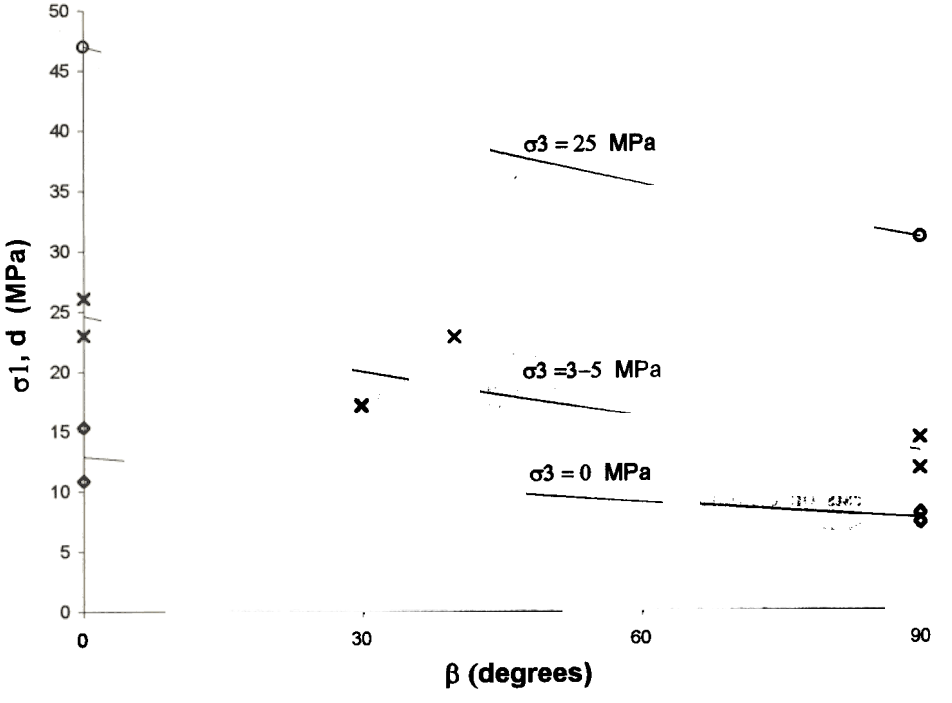

Figure 9. Influence of confining pressure and bedding plane orientation on axial stress at onset of dilation. Diamonds, σ_3 = 0 MPa; crosses, σ_3 = 3–5 MPa; circles, σ_3 = 25 MPa.

Table 2. Calculated Values of Relative Dilation

Sample	β, deg	P_c, MPa	$\Delta\sigma$, MPa	R^2	V_r, MPa
		0	16–16.7	0.8003	0.03087
		0	14.5–16.5	0.9633	0.03591
		3	20.5–22.4	0.9486	0.03190
		4.6	24–26.5	0.8998	0.01216
		10	15–18.5	0.9694	0.01844
		14.6	33–34	0.67117	0.02064
		25	23.5–24	0.649	0.01742
		3	21.5–24.5	0.975	0.0327
		3	23–25.5	0.949	0.02614
		0	14–16.5	0.9774	0.08241
		0	13–17	0.9776	0.09375
		3	16–23	0.9731	0.08111
		4.5	15–20	0.9829	0.04868
		24.7	17–22	0.9859	0.02881

β, bedding plane orientation; P_c, confining pressure; $\Delta\sigma$, stress difference interval used for linear regression; R^2, correlation coefficient.

purpose of demonstration. The effect of bedding plane orientation is more significant for parallel compression where the difference in relative dilation is about 3.2 ($(V_{\sigma_3=0}/V_{\sigma_3=25})_{\beta=90} \approx 3.2$), whereas in normal compression the difference is about 1.8 ($(V_{\sigma_3=0}/V_{\sigma_3=25})_{\beta=0} \approx 1.8$).

These observations indicate that for a fixed level of confining pressure, less mechanical energy is required to induce dilation as the major principal compressive stress direction becomes parallel with the discontinuities ($\beta \rightarrow 90°$). These findings should be valid for any transverse isotropic rock, but the effect is best demonstrated using rock salt due to its high sensitivity to small deviator stress changes. The practical implications of this finding are clear: in underground space created in transverse isotropic rock mass the rock is expected to dilate readily when the direction of anisotropy coincides with the direction of the major principal compressive stress. Furthermore, the relative dilation in parallel compression is expected to be much greater than in normal compression.

Applicability of Empirical Compression-Dilation Boundary Models

Several models have been published recently for the compression-dilation boundary in rock salt, some of which were reviewed by *Van Sambeek et al.* [1993]. *Cristescu and Hunsche* [1992], *Hunsche* [1993], and *Cristescu* [1993] reported true triaxial test results ($\sigma_1 > \sigma_2 > \sigma_3$) performed under fast loading rate on cubic specimens from Asse salt mine and Gorleben salt dome. *Spiers et al.* [1988] reported results from tests performed on cylindrical specimens of Asse salt under biaxial compression ($\sigma_1 > \sigma_2 = \sigma_3$) at constant strain rates. *Ratigan et al.* [1991] summarized the stress conditions which cause dilatancy of Avery Island domal salt and Waste Isolation Pilot Plant (WIPP) bedded salt in tests on cylindrical specimens under biaxial compression ($\sigma_1 > \sigma_2 = \sigma_3$). All three groups have attempted to generalize a compression-dilation boundary using stress invariant values taken at point of minimum volume.

The compression-dilation boundary of *Cristescu and Hunsche* [1992] has the form of a second-order polynomial:

$$\tau_{oct} \geq f_1\sigma_m^2 + f_2\sigma_m \tag{1}$$

where τ_{oct} is octahedral shear stress given by

$$\tau_{oct} = \frac{\sqrt{(\sigma_1 - \sigma_2)^2 + (\sigma_2 - \sigma_3)^2 + (\sigma_3 - \sigma_1)^2}}{3} \tag{2}$$

σ_m is mean or octahedral normal stress ($= (1/3)(\sigma_1 + \sigma_2 + \sigma_3) = (1/3)I_1$)

$$I_1 = 3\sigma_m$$

and their fitting parameters (for megapascals) are

$$f_1 = -0.0168, \qquad f_2 = 0.86$$

It can be shown that in terms of stress invariants the Cristescu and Hunsche criterion becomes

$$\sqrt{J_2} = -0.0023I_1^2 + 0.3511I_1 \tag{3}$$

where J_2 is the second invariant of the deviator stress tensor given by

$$\frac{[(\sigma_2 - \sigma_3)^2 + (\sigma_3 - \sigma_1)^2 + (\sigma_1 - \sigma_2)^2]}{6} \tag{4}$$

$$_{oct} = \sqrt{\frac{2J_2}{3}} \tag{5}$$

Spiers et al. [1988] have found a linear compression-dilation boundary of the form

$$\Delta\sigma \geq 2.74P + 6.4 \tag{6}$$

where P is the confining pressure ($\sigma_2 = \sigma_3$) and $\Delta\sigma$ is the difference between the axial stress and confining pressure ($\sigma_1 - \sigma_3$) in megapascals. In terms of stress invariants this criterion becomes [*Van Sambeek et al.*, 1993]

$$\sqrt{J_2} \geq 0.27I_1 + 1.9 \tag{7}$$

Finally, *Ratigan et al.* [1991] also suggest a linear boundary between compression and dilation, similar in form to the criterion of *Spiers et al.* [1988]:

$$\sqrt{J_2} \geq 0.27I_1 \tag{8}$$

Van Sambeek et al. [1993] plot the three criteria and argue that for low mean normal stress levels ($0 < I_1 < 50$ MPa; $0 < \sigma_m < 17$ MPa) the predictions are sufficiently similar for all criteria, and they proceed to develop a damage criterion for dilation initiation around underground openings in rock salt based on the *Ratigan et al.* [1991] boundary criterion. It should be noted, however, that for mean stresses greater than 20 MPa ($I_1 > 60$ MPa) the deviation between the polynomial expression of *Cristescu and Hunsche* [1992] and the two linear expressions is quite large.

The three boundary criteria are plotted in Figure 11 with all the data points which were obtained in this study. The results of both normal and parallel compression are shown. It can be seen that for $0 < I_1 < 60$ MPa the results, except for one outlier, fall within the band defined by the three criteria. However, for $I_1 > 60$ MPa a greater scatter is observed and a deviation from the linear rule is clearly suggested. Furthermore, when σ_1 is normal to bedding planes ($\beta = 0$), the boundary is higher then predicted by the suggested models, and follows roughly the criterion of *Spiers et al.* [1988]. Compression parallel to bedding planes ($\beta = 90$) roughly follows the model suggested by *Cristescu and Hunsche* [1992].

Best fit curves for our data are shown in Figure 12. Two curves are plotted for $\beta = 0$ (bold line) and for $\beta = 90$ (thin

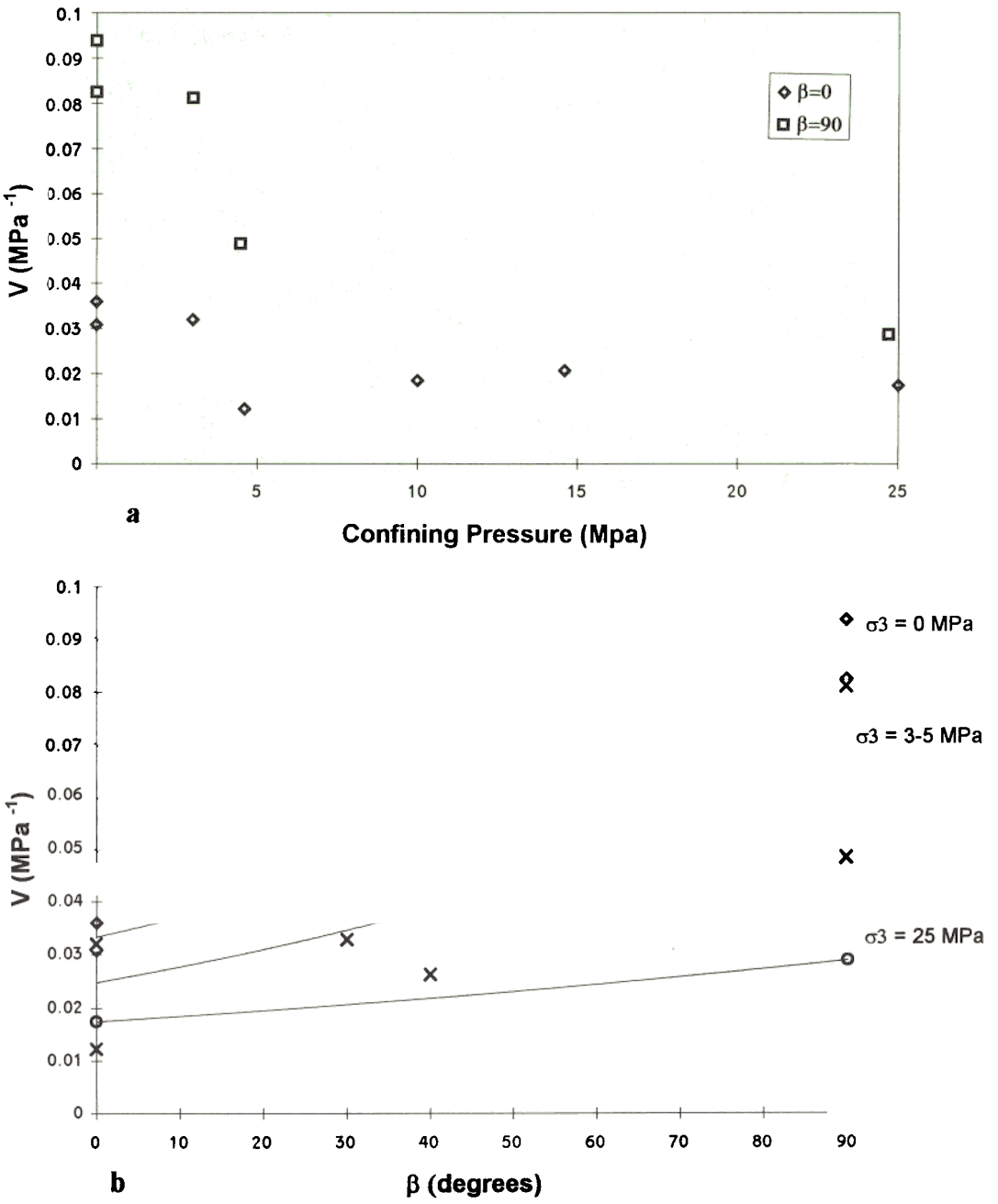

Figure 10. Sensitivity of relative dilation (V) to (a) confining pressure, and (b) bedding plane orientation. Diamonds, σ_3 = 0 MPa; crosses, σ_3 = 3–5 MPa; circles, σ_3 = 25 MPa. Correlation coefficient values (exponential fit) are R^2 = 0.98 (diamonds); R^2 = 0.67 (crosses); R^2 = 1 (circles).

line). A second-order polynomial equation provides the best approximation to the two data sets, yielding regression coefficients of 0.58. The polynomial form of the obtained boundaries is identical to that which was obtained by *Cristescu and Hunsche* [1992] for the general case (equation (1)) with value of fitting coefficients; see Table 3.

Several conclusions can be made from the discussion and observations above: (1) The compression-dilation boundary for normal compression (β = 0) is higher than for parallel compression (β = 90), (2) For low values of mean normal stress ($0 < \sigma_m < 17$ MPa) the boundary can be approximated by a linear law. For normal compression the boundary has an intercept with $(J_2)^{1/2}$ as found by *Spiers et al.* [1988]. The intercept value here is 2.9 MPa for normal compression only, and the intercept value suggested by *Spiers et al.* [1988] for their entire data set is 1.9 MPa. For parallel compression the intercept value is zero, as suggested by *Ratigan et al.* [1991], and by *Van Sambeek et al.* [1993] for the entire data set they analyzed. Two approximately linear boundaries should be used therefore for low mean normal stress, an upper boundary for normal compression (β = 0) with an intercept with $(J_2)^{1/2}$, and a lower boundary for parallel compression (β = 90) with intercept of 0, (3) For a large range of mean normal stress ($0 < \sigma_m < 33$ MPa) the compression-dilation boundary is defined by a second-order polynomial law as suggested by *Cristescu and Hunsche* [1992]. Two boundaries must be used,

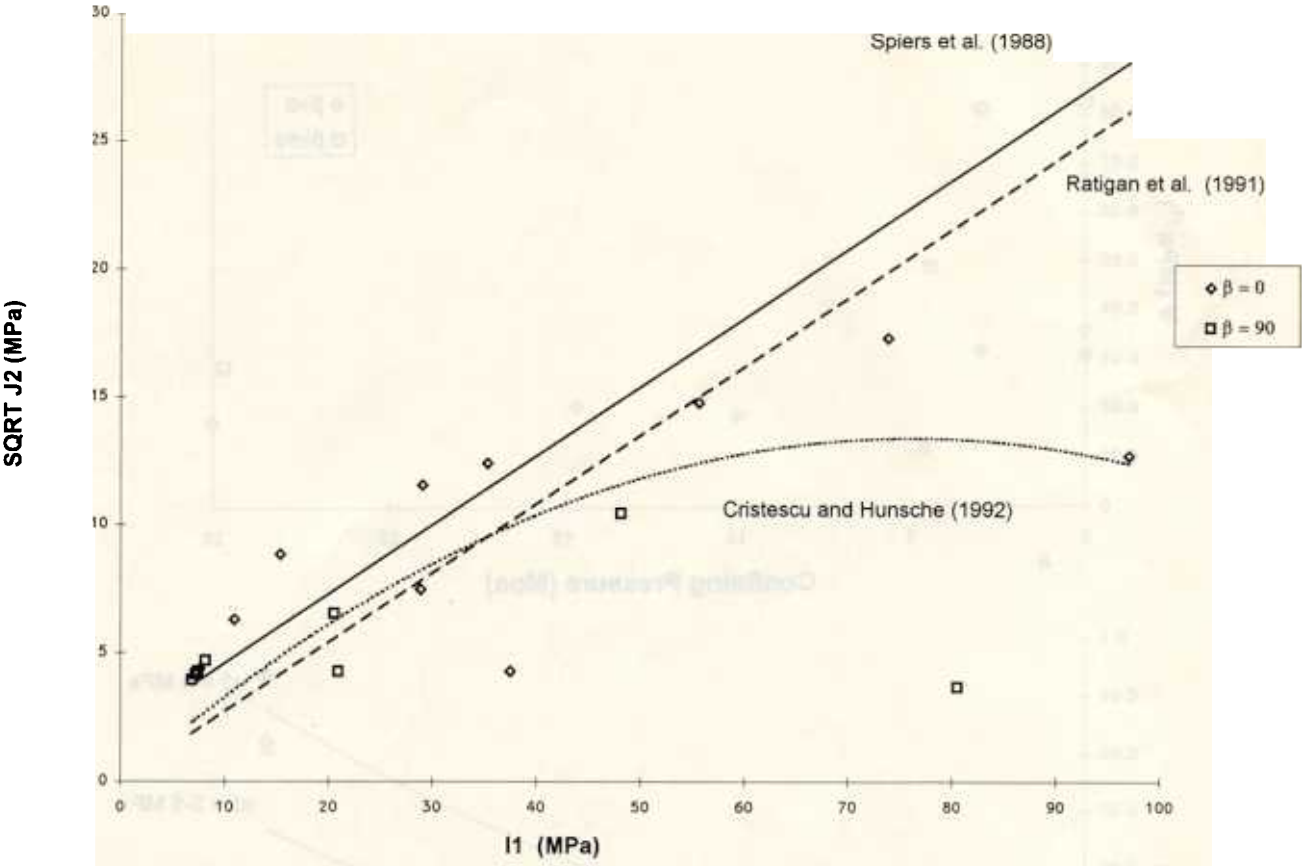

Figure 11. Recent models for compression-dilation boundary [after *Van Sambeek et al.*, 1993] and results of this study: diamonds, $\beta = 0°$; squares, $\beta = 90°$.

however: an upper boundary for $\beta = 0$ and a lower boundary for $\beta = 90$. It is expected that for inclined anisotropy ($0 < \beta < 90$) the results should plot between the two boundaries.

Discussion

Volume growth or dilation has recently become a major issue in the study of rock salt mechanics due to an increasing interest in utilization of underground space in rock salt for permanent storage of hazardous waste. Rock salt is a preferred candidate due to its high thermal conductivity, low water content, and very low permeability. The compression-dilation boundary is of particular interest, because once the stresses around an opening exceed that limit the rock is expected to dilate, microfracture processes are expected to ensue, and the permeability of the host rock is expected to increase.

The results presented above show that anisotropy should be considered in mechanical evaluation of rock salt behavior. It was shown that during linear-elastic deformation the effect of anisotropy is negligible, including the effect on yield stress. However, as soon as inelastic deformation develops and volume growth under compression ensues, anisotropy influences both stresses and rates of deformation. Some mechanical constraints on dilation in anisotropic rocks are discussed below, and a new empirical model for compression-dilation boundary in anisotropic rock salt is presented.

Constraints on Dilation in Anisotropic Rock

We have shown that bedding plane orientation has a pronounced effect on the compression-dilation boundary and evidently on the dilation mechanism. In brittle rock, which is inherently filled with initial flaws in the form of grain boundaries, the most commonly assumed mechanism for volume growth is the sliding crack model [*Brace and Bombalakis*, 1963; *Hoek and Bieniawski*, 1965; *Nemat-Nasser and Hori*, 1982; *Ashby and Hallam*, 1986; *Kemeny and Cook*, 1991]. In proposed solutions for the stress at crack initiation [e.g., *Ashby and Hallam*, 1986] the orientation of the initial flaw is a key factor, because the magnitudes of tensile stresses at a crack tip and shear stresses across a crack surface depend on crack orientation.

Volume growth has also been detected in ductile rock salts and potash salt rocks. *Van Sambeek et al.* [1993] reported measurements on initial voids before and after triaxial compression in rock salt using petrographic microscopy. They found that the vast majority of void volume was produced by a few relatively larger fractures and concluded that larger fractures grew preferentially after formation. A most important observation they made was that the fractures were always parallel or subparallel to the maximum principal stress and occurred almost exclusively on grain boundaries with few if any cleavage fractures. Similar findings were reported by *Lajtai et al.* [1994] who showed that tensile fractures in potash mines propagated parallel to the maximum principal stress trajectory (perpendicular to the minimum principal stress).

In the studied rock salts the matrix is quite homogeneous. The anisotropy, derived from sedimentation processes, is manifested by bedding plane partings. The preexisting bedding planes are also planes of discontinuity and as such are expected to be sites for nucleation and growth of dilation processes. The

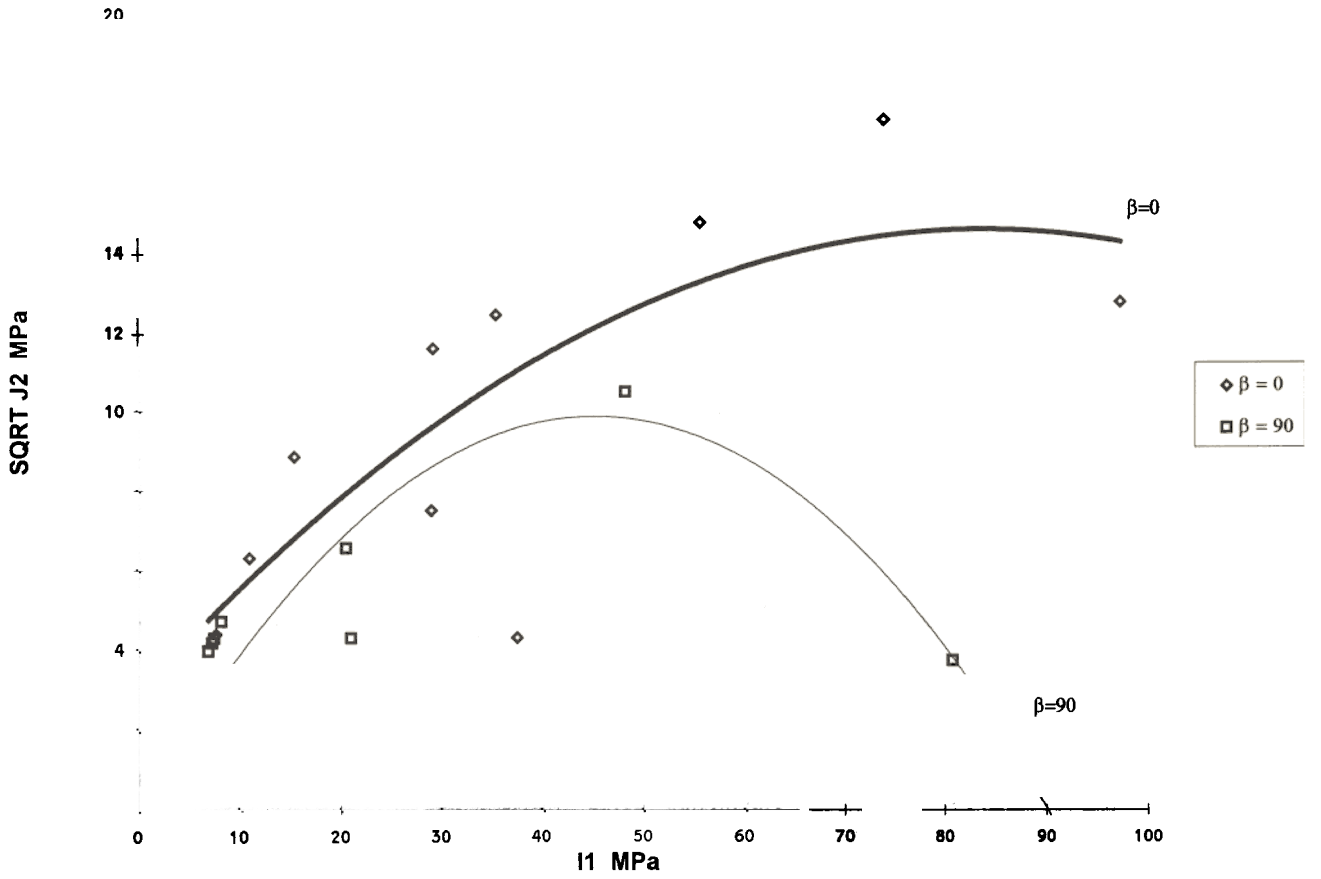

Figure 12. Best fit curves for compression-dilation boundary as found in this study: $\beta = 0$ bold line, $R^2 = 0.58$; $\beta = 90$ thin line, $R^2 = 0.58$.

energy required for dilation must overcome the force which keeps the dilating plane closed. The resultant compressive stress (p) which acts on an inclined plane in a biaxial compressive stress field generates the reaction against which dilation forces must act. The magnitude of p in terms of principal stresses is given by

$$P = \sqrt{\sigma_1^2 \cos^2 \beta + \sigma_2^2 \sin^2 \beta} \tag{9}$$

and the shear and normal stress components are

$$\tau = \frac{(\sigma_1 - \sigma_2) \sin 2\beta}{2} \tag{10}$$

$$\frac{\sigma_1 + \sigma_2}{2} \quad \frac{(\sigma_1 - \sigma_2) \cos 2\beta}{2} \tag{11}$$

Table 3. Comparison Between Second-Order Polynomial Coefficients Where Anisotropy Is Ignored [*Cristescu and Hunsche*, 1992] and Results of This Study for Parallel and Normal Compression

Cristescu and Hunsche's [1992] General Case	This Study	
	$\beta = 0°$	$\beta = 90°$
f_1 −0.0168	−0.0017	−0.0048
f_2 +0.86	+0.28	+0.44
Constant		

The magnitudes of the resultant stress vector p, the shear stress τ, and normal stress σ components are plotted in Figure 13 as a function of β, where β is the angle between the plane normal and σ_1, as defined above. At the two extreme orientations the magnitude of the resultant stress becomes equal to the magnitude of a principal stress. In normal compression, where $\beta = 0$, the magnitude of p equals to the major principal compressive stress (σ_1); in this configuration, maximum amount of energy is required for dilation, the onset of which is expected to take place at relatively high $\sigma_{1,d}$ values. In parallel compression, where $\beta = 90°$, the magnitude of p is equal to the minor principal compressive stress (σ_3); in this configuration the energy required for dilation is minimal, and onset of dilation is expected to take place at relatively low values of $\sigma_{1,d}$. In any other orientation the magnitude of p is between these two extreme values, depending on the value of β.

A New Empirical Model for Compression-Dilation Boundary in Anisotropic Rock Salt

The results of this study can be used for the determination of the major principal stress at onset of dilation ($\sigma_{1,d}$) as a function of confining pressure σ_3 and discontinuity orientation β by the following model:

$$\sigma_{1,d} = k_1 e^{k_2 \beta} \tag{12}$$

where k_1 is a function of σ_3 given by a second-order polynomial:

$$k_1 = -0.0743\sigma_3^2 + 3.2223\sigma_3 + 12.9$$

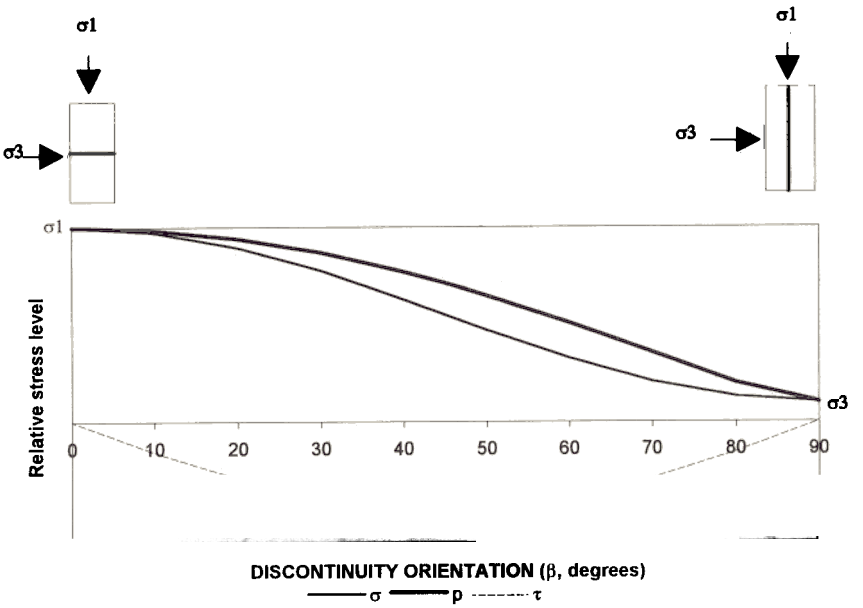

Figure 13. Influence of discontinuity orientation on the magnitude of the normal stress σ, shear stress τ, and stress vector p across a discontinuity plane.

and k_2 is a power coefficient. The values of k_1 and k_2 obtained in this study are given in Table 4. The power coefficient k_2 can be approximated by an average value of -0.0057. The predictive capability of the model is shown in Figure 14 where predicted and measured values of $\sigma_{1,d}$ are compared.

Having established the validity of the model (equation (12)) for our set of data (Figure 14), we proceed and create a generalized prediction for a range of discontinuity orientations ($0 \leq \beta \leq 90°$) and confining pressures ($0 \leq \sigma_3 \leq 25$ MPa), as shown in Figure 15. It can be seen that stress at onset of dilation decreases with increasing value of β. The rate of change of $\sigma_{1,d}$ with respect to β decreases with decreasing confining pressure, and the rate of change of $\sigma_{1,d}$ decreases with increasing confining pressure for all values of β.

Summary and Conclusion

The mechanical behavior of anisotropic rock salt is discussed using bedded rock salt samples which were extracted from Mount Sedom salt diapir. The stress-strain law of the tested samples consists of elastic, transition, and elastic-plastic stages of deformation. The strengthening effect of confining pressure is observed up to 4.5 MPa, beyond which little influence of pressure on the stress-strain law is detected. Confining pres-

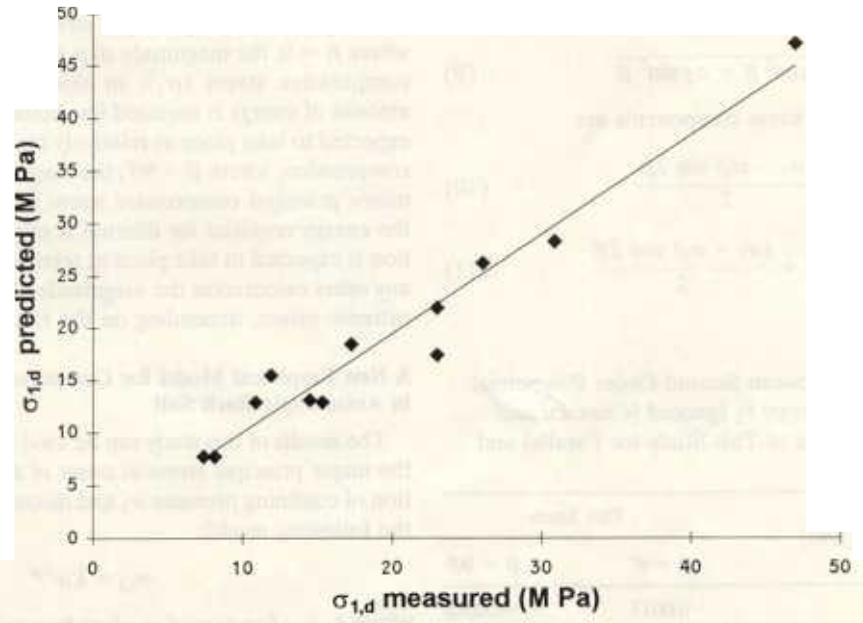

Figure 14. Correlation between empirical model predictions and observations for axial stress at onset of dilation ($R^2 = 0.956$).

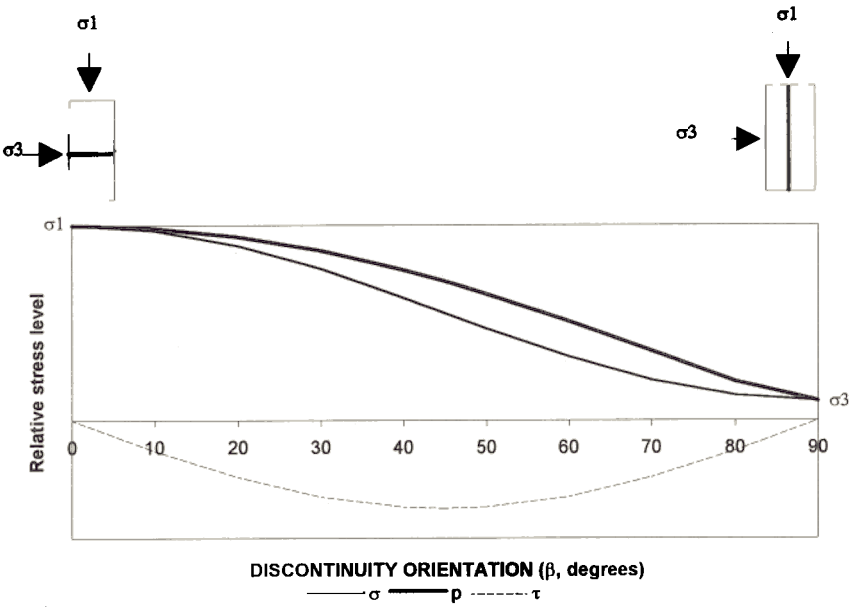

Figure 13. Influence of discontinuity orientation on the magnitude of the normal stress σ, shear stress τ, and stress vector p across a discontinuity plane.

and k_2 is a power coefficient. The values of k_1 and k_2 obtained in this study are given in Table 4. The power coefficient k_2 can be approximated by an average value of -0.0057. The predictive capability of the model is shown in Figure 14 where predicted and measured values of $\sigma_{1,d}$ are compared.

Having established the validity of the model (equation (12)) for our set of data (Figure 14), we proceed and create a generalized prediction for a range of discontinuity orientations ($0 \leq \beta \leq 90°$) and confining pressures ($0 \leq \sigma_3 \leq 25$ MPa), as shown in Figure 15. It can be seen that stress at onset of dilation decreases with increasing value of β. The rate of change of $\sigma_{1,d}$ with respect to β decreases with decreasing confining pressure, and the rate of change of $\sigma_{1,d}$ decreases with increasing confining pressure for all values of β.

Summary and Conclusion

The mechanical behavior of anisotropic rock salt is discussed using bedded rock salt samples which were extracted from Mount Sedom salt diapir. The stress-strain law of the tested samples consists of elastic, transition, and elastic-plastic stages of deformation. The strengthening effect of confining pressure is observed up to 4.5 MPa, beyond which little influence of pressure on the stress-strain law is detected. Confining pres-

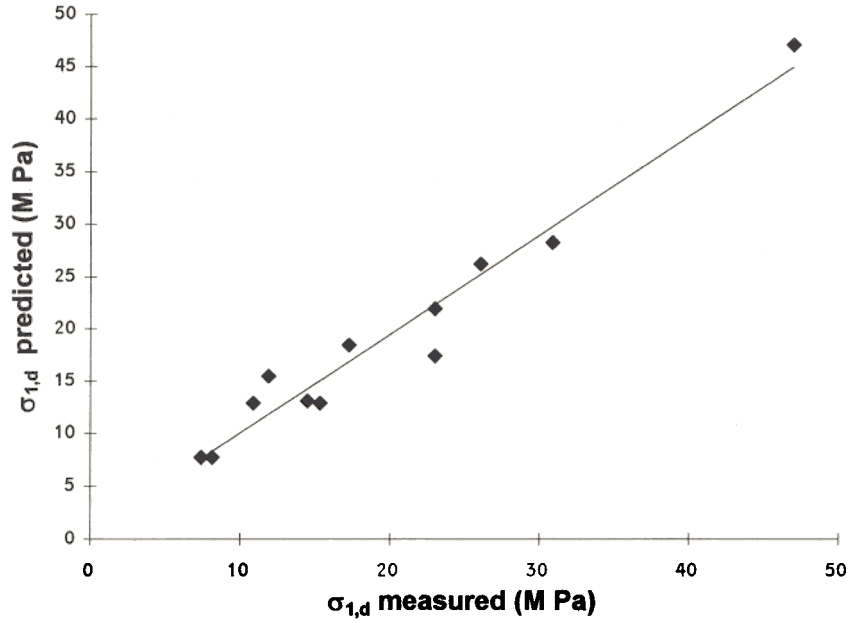

Figure 14. Correlation between empirical model predictions and observations for axial stress at onset of dilation ($R^2 = 0.956$).

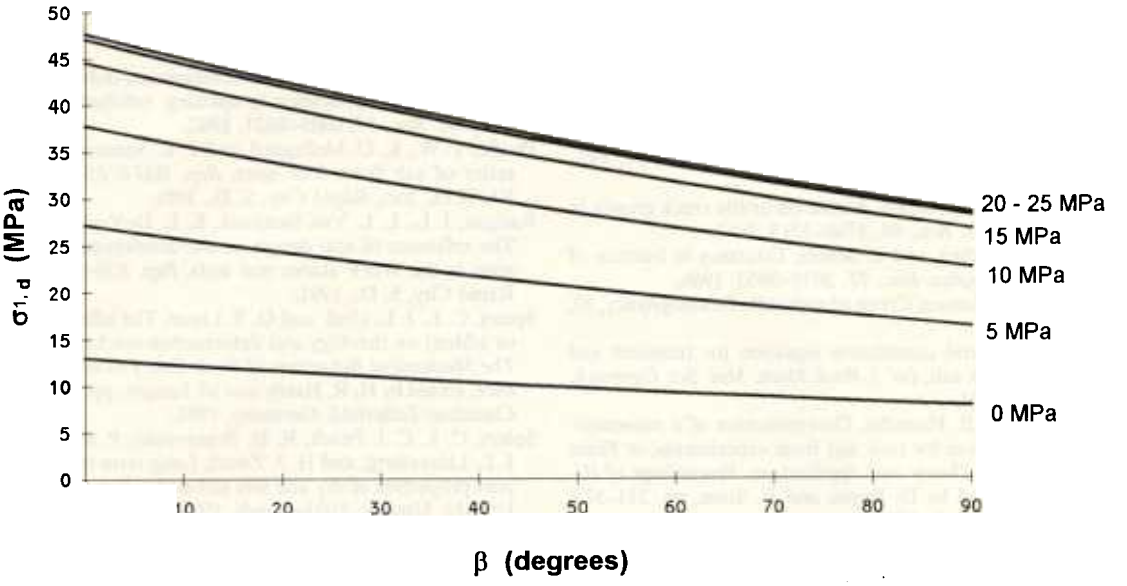

Figure 15. Model prediction for axial stress at onset of dilation as a function of confining pressure and bedding plane orientation.

sure increase during the elastic-plastic deformation stage has little effect on the stress-strain law. These features are characteristic of other rock salt bodies as well [e.g., *Wawersik and Hannum*, 1980].

The influence of anisotropy on the mechanical behavior is studied in terms of the stress-strain law, the elastic constants, the yield stress, and the compression-dilation boundary. Careful measurements of elastic modulus and Poisson's ratio indicate that they are influenced by confining pressure but insensitive to anisotropy. Similarly, yield stress is clearly influenced by confining pressure but not by anisotropy. The stress-strain curve therefore indicates isotropy at least up to the yield stress.

The volumetric strain curve indicates isotropy during the elastic stage of deformation, in agreement with the results discussed above, and up to onset of dilation. However, initiation of inelastic deformation (dilation) and relative volume growth are highly sensitive to anisotropy. The stress at onset of dilation depends on the orientation of the discontinuities: maximum stresses are measured when compression is normal to bedding planes ($\beta = 0°$), the stress decreases with increasing values of β, and minimum values are measured when compression is parallel to bedding planes ($\beta = 90°$). Similarly, the amount of compression prior to dilation decreases with increasing values of β. The influence of confining pressure on volumetric strain and on dilation follows typical trends of rock salt, for example, as shown by *Stormont et al.* [1992]. An important new observation is that the relative dilation ($V = |\Delta\varepsilon_v/\Delta(\sigma_1 - \sigma_2)|$, $\sigma_1 > \sigma_d$), defined beyond dilation point along the linear segment of the stress-volumetric strain curve, is highly sensitive to both confining pressure and anisotropy. Relative dilation increases with decreasing confining pressure and increasing β; namely, dilation is intensified with decreasing confining pressure and as the major principal compressive stress direction becomes parallel with the discontinuities (bedding planes).

Current models for the compression-dilation boundary ignore anisotropy and therefore provide site specific solutions but fail to describe general rock salt behavior. It is shown that the compression-dilation boundary should have the form predicted by *Cristescu and Hunsche* [1992]; however, a dual criterion must be used for normal and parallel compression ($\beta = 0$ and $\beta = 90$, respectively).

Using a very simple mechanistic approach and assuming that dilation processes nucleate inside the available discontinuities, it is argued that the work required for dilation is a function of β. In normal compression ($\beta = 0°$), dilation energy must overcome the magnitude of the resultant compressive stress across the discontinuity, which in that configuration is identical to the value of the maximum compressive stress (σ_1). In parallel compression ($\beta = 90°$) the magnitude of the resultant compressive stress equals the minor principal compressive stress (σ_3). Therefore the external energy required for dilation decreases with increasing β.

A new empirical model for dilation in anisotropic rock salt is developed for our specific data set of Mount Sedom samples. According to our site specific model predictions, stress at onset of dilation ($\sigma_{1,d}$) decreases with decreasing confining pressure and with increasing value of β. The rate of change of $\sigma_{1,d}$ with respect to β decreases with decreasing confining pressure, and the rate of change of $\sigma_{1,d}$ decreases with increasing confining pressure for all values of β.

Table 4. Experimentally Obtained Values of Empirical Coefficients k_1 and k_2

σ_3, MPa	k_1	k_2
0	14.9	−0.0047
4	24.6	−0.0068
25	47	−0.0057

Acknowledgments. This research is supported by Israel Ministry of Science and Arts through contract 6246-1-94 and 6246-2-95. The assistance of V. Palchik with the development of the empirical model is thankfully acknowledged. R. Weinberger produced Figures 1 and 2 and his help is thankfully acknowledged. The comments of D. F.

McTigue and another anonymous reviewer helped improve the flow of ideas which are conveyed in this publication.

References

Ashby, M. F., and S. D. Hallam, The failure of brittle solids containing small crack under compressive stress states, *Acta Metall., 34*, 497–510, 1986.

Brace, W. F., and E. G. Bombalakis, A note on brittle crack growth in compression, *J. Geophys. Res., 68*, 3709–3713, 1963.

Brace, W. F., B. W. Paulding, and C. Scholz, Dilatancy in fracture of crystalline rocks, *J. Geophys. Res., 71*, 3939–3953, 1966.

Carter, N. L., and F. D. Hansen, Creep of rock salt, *Tectonophysics, 92*, 275–333, 1983.

Cristescu, N. D., A general constitutive equation for transient and stationary creep of rock salt, *Int. J. Rock Mech. Min. Sci. Geomech. Abstr., 30*, 125–140, 1993.

Cristescu, N. D., and U. E. Hunsche, Determination of a nonassociated constitutive equation for rock salt from experiments, in *Finite Inelastic Deformation—Theory and Applications, Proceedings of IUTAM Symposium*, edited by D. Besdo and E. Stein, pp. 511–523, Springer-Verlag, New York, 1992.

Djahanguiri, F., and S. C. Matthews, Geotechnical considerations for design of nuclear repository in bedded salt in the U.S., in *Proceedings of the Six International Symposium on Salt*, vol. 1, pp. 561–584, Salt Inst., Phoenix, Ariz., 1983.

Frumkin, A., Uplift rate relative to base-levels of a salt diapir (Dead Sea Basin, Israel) as indicated by cave levels, in *Salt Tectonics*, edited by G. I. Alsop, D. J. Blundell, and I. Davison, Geol. Soc. Spec. Publ., *100*, 41–47, 1996.

Hansen, F. D., K. D. Mellegard, and P. E. Senseny, Elasticity and strength of ten natural rock salts, in *The Mechanical Behaviour of Rock Salt, Proceedings of 1st Conference*, edited by H. R. Hardy and M. Langer, pp. 71–84, Trans Tech, Clausthal-Zellerfeld, Germany, 1981.

Hoek, E., Strength of jointed rock, *Geotechnique, 33*, 187–223, 1983.

Hoek, E., and Z. T. Bieniawski, Brittle fracture propagation in rock under compression, *Int. J. Fract. Mech., 1*, 139–155, 1965.

Hunsche, U. E., Failure behaviour of rock salt around underground cavities, in *7th International Symposium on Salt*, vol. I, pp. 59–65, Elsevier, New York, 1993.

Jaeger, J. C., and N. G. W. Cook, *Fundamentals of Rock Mechanics*, 3rd ed., 593 pp., Chapman and Hall, New York, 1979.

Kemeny, J. M., and N. G. W. Cook, Micromechanics of deformation in rocks, in *Toughening Mechanisms in Quasi-Brittle Materials*, edited by S. P. Shah, pp. 155–188, Kluwer Acad., Norwell, Mass., 1991.

Lajtaji, E. Z., B. J. Carter, and J. S. Duncan, En echelon crack-arrays in potash salt rock, *Rock Mech. Rock Eng., 27*, 89–111, 1994.

Langer, M., Geotechnical investigation methods for rock salt, *Bull. Int. Assoc. Eng. Geol., 25*, 155–164, 1982.

Martin, C. D., and N. A. Chandler, The progressive fracture of Lac du Bonnet Granite, *Int. J. Rock Mech. Min. Sci. Geomech. Abstr., 31*, 643–659, 1994.

Nemat-Nasser, S., and H. Hori, Compression-induced nonplanar crack extension with application to splitting, exfoliation and rockburst, *J. Geophys. Res., 87*, 6805–6821, 1982.

Pfeifle, T. W., K. D. Mellegard, and P. E. Senseny, Constitutive properties of salt from four sites, *Rep. RSI-0165 ONWI-314*, 84 pp., RE/SPEC Inc., Rapid City, S. D., 1981.

Ratigan, J. L., L. L. Van Sambeek, K. L. DeVries, and J. D. Nieland, The influence of seal design on the development of disturbed rock zone in the WIPP alcove seal tests, *Rep. RSI-0400*, RE/SPEC Inc., Rapid City, S. D., 1991.

Spiers, C. J., J. L. Urai, and G. S. Lister, The effect of brine (inherent or added) on rheology and deformation mechanisms in salt rock, in *The Mechanical Behaviour of Rock Salt, Proceedings of 2nd Conference*, edited by H. R. Hardy and M. Langer, pp. 89–102, Trans Tech, Clausthal-Zellerfeld, Germany, 1984.

Spiers, C. J., C. J. Peach, R. H. Brzesowsky, P. M. T. M. Schutjensm, J. L. Liezenberg, and H. J. Zwart, Long term rheological and transport properties of dry and wet salt rocks, *Rep. EUR 11848*, Univ. of Utrecht, Utrecht, Netherlands, 1988.

Stormont, J. C., and J. J. K. Daemen, Laboratory study of gas permeability changes in rock salt during deformation, *Int. J. Rock Mech. Min. Sci. Geomech. Abstr., 29*, 325–342, 1992.

Stormont, J. C., J. J. K. Daemen, and C. S. Desai, Prediction of dilation and permeability changes in rock salt, *Int. J. Numer. Anal. Methods Geomech., 16*, 545–569, 1992.

Van Sambeek, L. L., J. L. Ratigan, and F. D. Hansen, Dilatancy of rock salt in laboratory tests, *Int. J. Rock Mech. Min. Sci. Geomech. Abstr., 30*, 735–738, 1993.

Wawersik, W. R., and D. M. Hannum, Mechanical behavior of New Mexico salt in triaxial compression up to 200°C, *J. Geophys. Res., 85*, 891–900, 1980.

Zak, I., The geology of Mount Sedom, Ph.D. thesis, Hebrew Univ., Jerusalem, 1967.

Zak, I., and R. Freund, Strain measurements in eastern marginal shear zone of Mount Sedom salt diapir, Israel, *AAPG Bull., 64*, 568–581, 1980.

Y. H. Hatzor and E. P. Heyman, Deichmann Rock Mechanics Laboratory of the Negev, Department of Geological and Environmental Sciences, Ben-Gurion University, Beer-Sheva, 84105, Israel. (e-mail: hatzor@bgumail.bgu.ac.il)

(Received October 4, 1996; revised March 17, 1997; accepted March 28, 1997.)